ELSEVIER

NDT&E International 35 (2002) 317–328

NDT&E international

www.elsevier.com/locate/ndteint

Propagation of guided waves in adhesive bonded components

Robert Seifried[a,1], Laurence J. Jacobs[a,*], Jianmin Qu[b]

[a]School of Civil and Environmental Engineering, Georgia Institute of Technology, Atlanta, GA 30332-0355, USA
[b]G.W. Woodruff School of Mechanical Engineering, Georgia Institute of Technology, Atlanta, GA 30332, USA

Received 26 June 2001; revised 15 October 2001; accepted 25 October 2001

Abstract

The objective of this research is to use analytical and computational models to develop a quantitative understanding of the propagation of guided Lamb waves in multi-layered, adhesive bonded components. Key issues of this study include the effect of the adhesive bond layer, including its low stiffness (relative to the adherends) and viscoelastic behavior. The propagation of these guided waves are interpreted in terms of dispersion relationships, displacement profiles and attenuation curves (both as functions of frequency and wavenumber). The ultimate goal of this study is to determine the effectiveness and sensitivity of guided Lamb waves to determine the in situ properties of an adhesive bond. A combination of the analytical model, transient FEM simulation and experimental measurements provides a better understanding of the guided wave's behavior in this layered waveguide.

Keywords: Lamb waves; Adhesive; Frequency–wavenumber

1. Introduction

A promising new methodology uses guided ultrasonic waves to interrogate adhesive bonded components; the primary advantage of using guided waves in this application is that they are capable of interrogating large, inaccessible components in a time-efficient manner. The main difficulty with using guided waves is the inherent complexity of the waveforms, making interpretation difficult. Previous research [1] combined laser ultrasonic techniques with the two-dimensional Fourier transformation (2D-FFT) to experimentally characterize the stiffness of adhesive bonds with guided Lamb waves (Lamb waves are guided plate waves). This research experimentally measured transient waves in three-layer (two aluminum plate adherends joined by an adhesive) and two-layer (the same aluminum plate bonded to the same, single adhesive layer) plate specimens, to study the influence of the adhesive bond on the dispersion curves of these specimens.

These experimental results [1] show that the modes excited and measured in these bonded specimens are always identical to the dispersion curves of a single plate—one of the aluminum adherends. When the adhesive bond's stiffness is low in comparison to the adherend's stiffness, the specimen behaves like a single stress free plate of the thickness of the independent plate components. For example, Fig. 1 shows the experimentally measured dispersion curves (contour plot of the three-dimensional frequency versus wavenumber spectrum) for a three-layer bonded specimen—two 0.9398 mm thick aluminum plate adherends joined with a 0.25 mm thick adhesive layer. These experimentally measured contours are superimposed on the theoretical solution (solid lines) of the Rayleigh–Lamb frequency spectrum for a single aluminum plate with a thickness of 0.9398 mm (one of the adherends). Additional experimental insights are that the number of modes measured in the two- and three-layer bonded specimens is always less than the number of modes measured in a single, stress free plate. Both the two- and three-layer bonded specimens behave like a single plate (one of the adherends), there are just fewer modes observed in these bonded specimens. In addition, the modes measured in a bonded specimen are less defined (less clarity), and generally exist through a smaller frequency (or wavenumber) bandwidth than those measured in the corresponding, single plate. In summary, the adhesive layer does not cause any frequency shifts in the dispersion curves (in comparison to a single plate), but it does damp-out portions of these modes—see Ref. [1] for details.

The objective of the current research is to use analytical and computational models to develop a quantitative

* Corresponding author. Tel.: +1-404-894-2771; fax: +1-414-894-0211.
E-mail address: ljacobs@ce.gatech.edu (L.J. Jacobs).
[1] Current address: Institute B of Mechanics, University of Stuttgart, Stuttgart, Germany.

0963-8695/02/$ - see front matter
PII: S0963-8695(01)00056-1

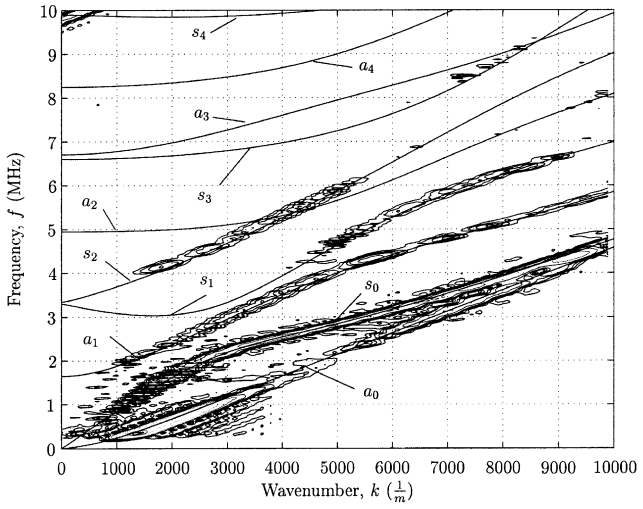

Fig. 1. Typical experimentally measured dispersion curves of the three-layer model, plus analytical dispersion curves of a single aluminum plate adherend (solid lines).

understanding of the propagation of guided Lamb waves in multi-layered, adhesive bonded components. A specific goal of this study is to develop a theoretical understanding of the experimental behavior observed in Ref. [1]. Key issues of this study include the effect of the adhesive bond layer, including its low stiffness (relative to the aluminum adherends) and its viscoelastic behavior. The propagation of these guided waves are interpreted in terms of dispersion relationships, displacement profiles and attenuation curves (both as functions of frequency and wavenumber). The ultimate goal of this study is to determine the effectiveness and sensitivity of guided Lamb waves to determine the in situ properties of an adhesive bond.

The analytical model (developed following Ref. [2]) describes the steady-state solution of guided waves in layered media. This steady-state solution is a frequency–wavenumber relationship for the different modes that can propagate in layered media and is presented in the form of dispersion curves. The corresponding displacement fields are calculated by solving for the eigenvectors (for a particular wavenumber) of the associated eigenvalue problem (the dispersion relationship). The adhesive bonds investigated in this research are polymers, which are viscoelastic materials. This viscoelastic behavior causes amplitude damping and frequency shifts as a guided wave propagates in an adhesive bonded component. This study assumes a Kelvin–Voight solid, and a linearization (needed to simplify complex root solving) to describe the frequency-dependent attenuation of the adhesive layer. The resulting attenuation of each mode is calculated in order to determine which modes are damped out, and at which frequencies.

The solution of the analytical model, with its dispersion curves, displacement fields and attenuation curves explain most, but not all of the experimentally observed phenomena. These analytical models cannot determine absolute amplitudes of the individual modes in the dispersion curves, yet these amplitudes are exactly the quantity measured in the experiments [1]. So, this research applies the finite element (FEM) code, ABAQUS/Explicit, to numerically model the transient, Lamb wave propagation problem. This FEM simulation is very robust, producing an enormous amount of data (such as the time-dependent displacements at multiple locations, including interior points) in a single 'numerical experiment'. A combination of the analytical model, transient FEM simulation and experimental measurements provides an excellent understanding of the guided wave's behavior in an adhesive bonded, layered waveguide.

Lowe and Cawley [3] analyzed the sensitivity of adhesive bond properties on guided waves using a three-layer model, and showed that Lamb waves are strongly sensitive to the material properties and thicknesses of the adherends, while being very insensitive to the properties of the adhesive bond. Their results are similar to those of Nagy and Adler [4], who studied guided waves in adhesive layers between two half-spaces, and demonstrated that the resulting dispersion curves are relatively insensitive to the properties of the adhesive layer. Lowe et al. [5] recently used the FEM to study the transmission of Lamb waves across adhesively bonded lap joints, demonstrating the physics of the mode conversion behavior and providing a basis for the selection of modes for NDE of bonds. In addition, a number of researchers have developed dispersion curves using oblique incidence measurements with immersion piezoelectric transducers (e.g. see Ref. [6]).

2. Analytical model: elastic case

Previous researchers such as Pavlakovic et al. [7] and Niklasson and Datta [8] have developed analytical models for layered elastic plates. In a similar fashion, the current research develops an analytical model for guided waves in layered plates and uses this model to gain insights into the experimental behavior observed in Ref. [1]. In brief (and following Ref. [2]), this model uses potential functions to separately describe the steady-state (harmonic) solution of the governing wave equations for each layer (plane-strain, elastic and isotropic material). The resulting displacement and traction components for each layer are written in terms of four arbitrary constants (four constants for each layer). In general, an N-layer specimen requires $4N$ boundary (or continuity) conditions to evaluate the constants. The specimens under consideration in this research have the following boundary conditions:

- The upper and lower surfaces are stress free, so the tractions σ_{22} and σ_{12} are zero at these locations.
- Continuity of displacement and stress at each interface, so the tractions σ_{22} and σ_{12} and displacements u_1 and u_2 in each layer are equal at the interfaces.

The resulting system of 12 homogeneous equations for

the three-layer specimen (or eight homogeneous equations for the two-layer case) is written in matrix form, and the condition that the determinant of this matrix must vanish yields a characteristic equation that is solved numerically with a FORTRAN program. The 12 homogeneous equations of the three-layer case are presented in Appendix A, and details on the numerical procedure are available in Ref. [9].

The eigenvalues for this characteristic equation are the frequency–wavenumber (f–k) relationships of the different modes, while the associated eigenvectors are the displacement fields for each mode. Because the frequency of a mode is a function of wavenumber, each point on the mode has a different eigenvector, and thus a different displacement field. For any pair of f–k values of a mode, the associated eigenvectors can be calculated by plugging them back into the eigen-problem and solving the resulting linear system. The eigenvectors can only be calculated up to an arbitrary constant, so it is helpful to normalize the displacement field to the maximum displacement. This normalization leads to an qualitative description of the displacement field—a quantitative statement about the amplitudes of the displacement field is not possible. Finally, the correctness and accuracy of the current analytical model (and its associated numerical solution) is tested by benchmarking with the results of a three-layer model published in Ref. [3]—there is excellent agreement between the two procedures see Ref. [9] for details.

Now consider a three-layer bonded specimen of two aluminum plate adherends, joined together with an adhesive layer (the middle layer) with properties similar to the specimens examined in Ref. [1]. Each aluminum plate is 0.9398 mm thick, while the adhesive layer is 0.25 mm thick. The aluminum has a longitudinal wave speed of 6450 m s^{-1}, a shear wave speed of 3100 m s^{-1} and a density of 2700 kg m^{-3}, while the adhesive properties are taken as longitudinal wave speed of 771 m s^{-1}, shear wave speed of 370 m s^{-1} and a density of 1106 kg m^{-3}. Note that the wave speeds for the adhesive layer (used in this three-layer analytical model) are higher than those mentioned in Ref. [1]—the stiffness values presented in Ref. [1] are the static stiffness values provided by the adhesive manufacturer. These stiffnesses were only presented in Ref. [1] for reference purposes and were not used in any calculations. In reality, the adhesive will be much stiffer at the ultrasonic frequencies considered in this study. In fact, the adhesive will respond as a glassy material at these higher frequencies, and will be significantly stiffer than in the static (rubbery) range, see Ref. [10] for details on the behavior of wave propagation in polymers. The wave speeds used in this paper for the adhesive layer are a reasonable representation of the actual wave speeds measured in Ref. [1]. Note that a lower stiffness material has also been studied (with this same model, see Refs. [9,11] for details), yielding the same general behavior that will be presented in the following sections. In addition, the influence of the frequency dependency of the viscoelastic adhesive layer is discussed in Section 3.

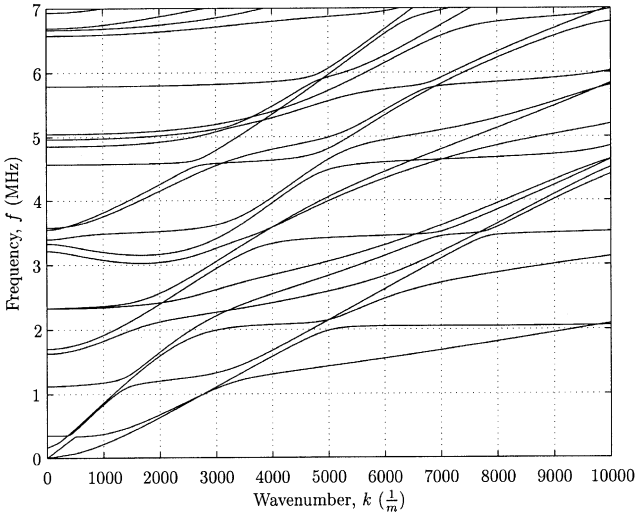

Fig. 2. Analytical dispersion curves for the three-layer model.

Fig. 2 shows the analytically calculated dispersion curves for the three-layer model in a wavenumber range of 0–10 000 m^{-1} and a frequency range of 0–7 MHz—Fig. 2 is the analytical representation of the experimentally measured dispersion curves shown in Fig. 1. First, the analytical solution shows many more modes than are present in the experimental results of Fig. 1, for the same three-layer specimen. The analytical model shows about 20 more modes (many that have substantial, nearly horizontal portions) that are not measured in the experiments—these 'additional' modes do not appear in Fig. 1. The analytical solution (Fig. 2) also shows another significant feature—some modes seem to follow the modes of a single aluminum plate (one of the adherends). This is especially important when considering that the only experimentally observed modes in Fig. 1 are the single aluminum plate modes. In order to explain this behavior, Fig. 3 is a zoom of the dispersion curves in Fig. 2 (as dashed lines) for a wavenumber range of 0–5000 m^{-1} and a frequency range of 0–3 MHz, with the addition of the dispersion curves of a single aluminum plate (0.9398 mm thick—one of the adherends) noted as solid lines. This *artificial superposition* of the dispersion curves of a single aluminum plate (solid lines) onto the three-layer dispersion curves (dashed lines) in Fig. 3 is done as a visual aid for the following explanation. Fig. 3 shows that the modes that appear to be single aluminum plate modes are not individual modes (they are not continuous), but are composed of a series of different modes that merge to 'follow' the single aluminum plate modes for short wavenumber/frequency 'distances'. In general, two three-layer modes merge when following a single aluminum plate mode—these portions of the three-layer modes that follow a single aluminum plate mode are identified as 'aluminum modes' in the reminder of this paper.

As an explanation of this behavior, Fig. 4 presents the in-plane displacement components (u_1) plotted as solid lines, and the out-of-plane displacement components (u_2)

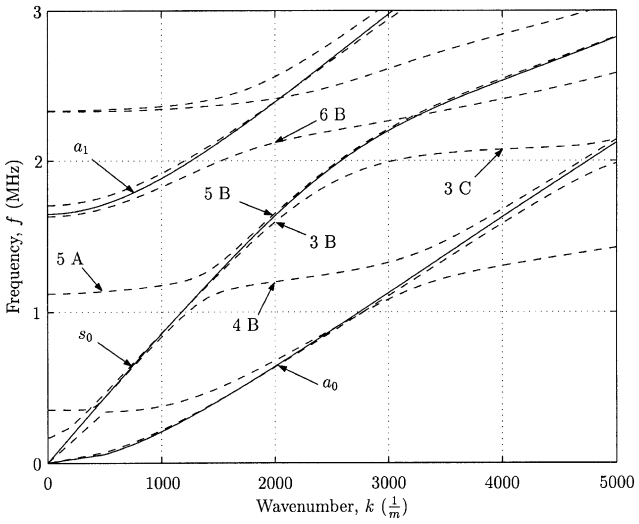

Fig. 3. Zoom of dispersion curves in Fig. 2, plus artificial superposition of single aluminum plate adherend (solid lines).

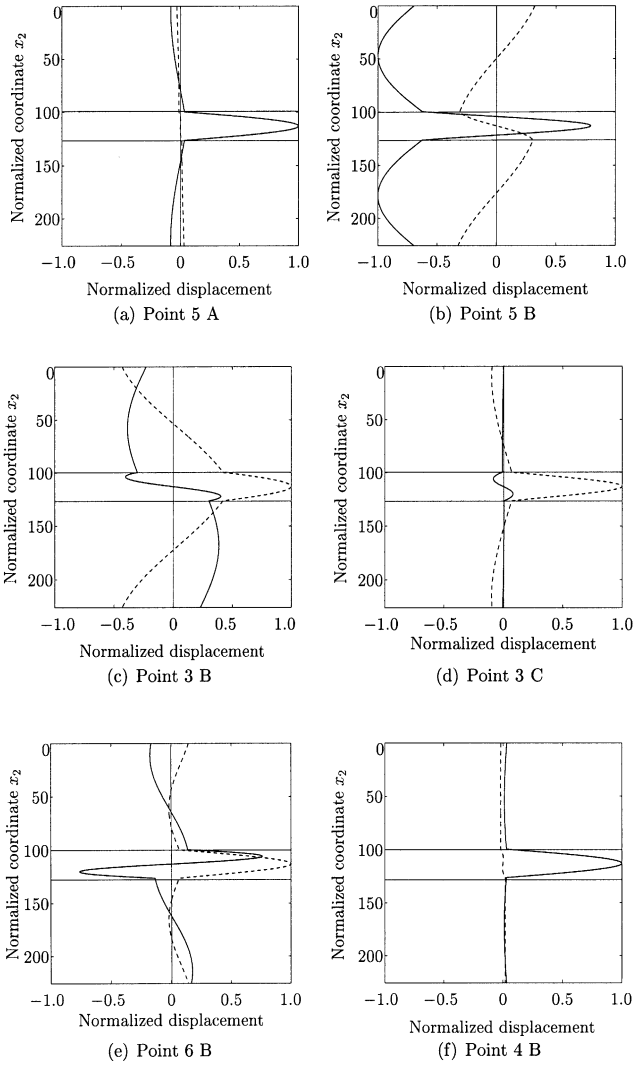

Fig. 4. Displacement fields (solid line in-plane and dashed line out-of-plane) for f–k locations identified in Fig. 3.

plotted as dashed lines at six different f–k pairs, whose locations are identified in Fig. 3. The vertical axes in Fig. 4 are the thicknesses of the entire three-layer specimen in the x_2 direction (through thickness), normalized to the thickness of a single aluminum plate (adherend)—one aluminum plate thickness (0.9398 mm) is equal to 100. The horizontal axes show the normalized displacements. Consider the displacements at points 5A (Fig. 4(a)) and 5B (Fig. 4(b)), two points on the same mode, one removed from the single aluminum plate mode (5A) and the other in the vicinity of this single plate mode (5B). Fig. 4(a) shows that the only significant displacements at 5A are in the adhesive layer—there is practically no displacement in the aluminum plates at 5A. In contrast, Fig. 4(b) shows that point 5B has substantial displacements in the adhesive layer *and* the aluminum plate layers. The displacements in the aluminum plates (high stiffness) dominate the displacements in the adhesive layer (low stiffness) at point 5B, so regions with significant displacements in the aluminum layers will have 'associated' displacements in the adhesive layer. This same behavior is evidenced when considering points 3B and 3C—two points on a different mode, one near, and one removed from the single plate mode (see Fig. 4(c) and (d)). An additional demonstration of this behavior is seen by comparing four points with the same wavenumber ($k = 2000\ \mathrm{m}^{-1}$), but on different modes (points 3B, 4B, 5B and 6B). There are only substantial displacements in the aluminum plate adherends of the three-layer model at this wavenumber for frequencies associated with a single aluminum plate mode (3B and 5B). This particular mode corresponds to the s_0 mode of a single aluminum plate. The shapes of the displacement fields at 3B and 5B in the aluminum layers of the three-layer model are similar to the displacement fields of a single aluminum plate, when examining the s_0 mode at the same f–k point. The displacement field of the s_0 mode in a single aluminum plate (0.9398 mm thick) at $k = 2000\ \mathrm{m}^{-1}$ is shown in Fig. 5 for confirmation. Finally, note that the displacement behavior discussed here is representative of nearly all the modes of this three-layer model, see Ref. [9] for details.

Since the experimental procedure (the laser interferometric detector of [1]) only measures out-of-plane

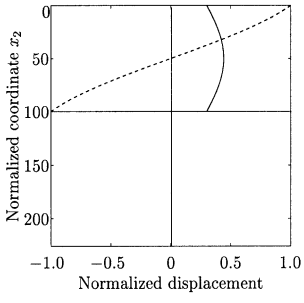

Fig. 5. Displacement fields (solid line in-plane and dashed line out-of-plane) for the s_0 mode of a single aluminum plate adherend at $k = 2000\ \mathrm{m}^{-1}$.

displacements on the outer surface of the three-layer bonded specimen, the experimental results of Fig. 1 are indicative of modes that have large out-of-plane displacements at the top and bottom surfaces of this three-layer bonded specimen. The three-layer analytical model results show that only f–k pairs in the vicinity of the single aluminum plate modes have substantial displacements (both in-plane and out-of-plane) on the surface of each aluminum plate adherends. As a result, the experimental measurements in Ref. [1] will only 'see' these aluminum modes—this is one reason why the experimental results for a three-layer bonded specimen in Fig. 1 only show (some of) the modes of a single, 0.9398 mm thick aluminum plate.

The dispersion results for a two-layer model (a single 0.9398 mm aluminum plate bonded to the same adhesive layer) show similar behavior as the three-layer model (see Refs. [9,11] for details on the two-layer model). The main difference is that the two-layer model always has only one mode following the aluminum mode—as opposed to the two modes that generally follow the aluminum mode in the three-layer model. As a result, the two aluminum plates of the three-layer model can combine (in-phase) to cause motion along the aluminum mode, while the two-layer model only has one aluminum plate to contribute to this motion. Consider the displacements at two points at the same aluminum mode, 3B and 5B in Fig. 4 as an illustration. Point 5B has in-phase, in-plane displacements, and out-of-phase, out-of-plane displacements, while 3B has the opposite—out-of-phase, in-plane displacements and in-phase, out-of-plane displacements. In contrast, the analogous two-layer specimen does not have a second plate which can combine (in-phase or out-of-phase) with the first plate. This contributes to the experimentally observed behavior of amplitudes in the two-layer specimen being smaller than the three-layer specimen [1].

3. Analytical model: viscoelastic case

The three-layer analytical model developed in Section 2 does not account for any viscoelastic behavior that can occur in the (polymer) adhesive layer. The adhesive's viscoelasticity causes material damping, and the accompanying amplitude attenuation. Most research in the field of attenuation of guided waves has concentrated on the *leakage* of wave energy from a solid waveguide into a viscous fluid [12]. Many authors define attenuation as the energy loss due to the leakage from one media (layer) into another [3], as opposed to losses due to material damping. In contrast, the current study defines attenuation as the amplitude loss solely due to material damping in the viscoelastic adhesive layer (the experiments of Ref. [1] used laser ultrasonic techniques, so the specimens are not immersed in a fluid). Previous researchers who studied the behavior of guided waves in viscoelastic materials mainly limited themselves to waves propagating in a single layer, see Refs. [13–15]. A recent publication [16] provides a theoretical prediction of the damping effect in a viscoelastic bond (layer), with an upper frequency limit of 2 MHz, for the first two modes.

The current research uses the Kelvin–Voight model (a parallel combination of a spring and a dashpot) to describe the viscoelastic material behavior of the adhesive bond layer. The stress–strain relationship for a Kelvin–Voight solid is given by

$$\sigma_{ij} = C_{ijkl}\varepsilon_{kl} + C'_{ijkl}\dot{\varepsilon}_{kl}. \tag{1}$$

The first term in Eq. (1) is the linear elastic contribution (the spring), while the second term is the viscous contribution (dashpot). As is the case for the linear elastic model of Section 2, assume a time harmonic function for strain and stress (e.g. $\varepsilon = \hat{\varepsilon}\, e^{i\omega t}$), and Eq. (1) becomes

$$\hat{\sigma}_{ij} = \tilde{C}_{ijkl}\hat{\varepsilon}_{kl}, \tag{2}$$

where $\tilde{C}_{ijkl}$ is the complex material modulus, defined as $\tilde{C}_{ijkl} = C_{ijkl} + i\omega C'_{ijkl}$. The viscoelastic stress–strain relationship in the harmonic case (Eq. (2)) is similar to the linear elastic stress–strain relationship, except that the material modulus is complex and frequency-dependent in the viscoelastic case—this similarity is known as the 'correspondence principle'. The real part of the material modulus $\tilde{C}$ corresponds to the material's capacity to store energy, while the imaginary part corresponds to the loss of energy in the material. The complex material modulus for an isotropic material is described with two independent moduli

$$\tilde{D} = d + i\omega d', \tag{3}$$

$$\tilde{S} = s + i\omega s', \tag{4}$$

where the modulus $\tilde{D}$ corresponds to the dilatation modulus in the linear elastic case, and the modulus $\tilde{S}$ corresponds to the shear modulus in the linear elastic case [13]. Note that the real parts of the moduli $\tilde{D}$ and $\tilde{S}$ are given by the linear elastic constants $d = \lambda + 2\mu$ and $s = \mu$, and are coupled by the Poisson's ratio, ν. A similar parameter is used to develop a relationship between the viscous material constants, d' and s'

$$\nu' = \frac{d'}{(2 - s')(d' - s')}. \tag{5}$$

The parameter ν' is similar to the Poisson's ratio ν, and has values between 0.5 and -1.0. A material where all the losses are due to shear deformation has $\nu' = -1.0$, while a material with no losses due to shear deformation has $\nu' = 0.5$.

The wavenumber k has a complex value in the viscoelastic case

$$k = k_r + ik_i. \tag{6}$$

This complex wavenumber yields an in-plane displacement (in the nth layer) in the form

$$u_1^{(n)} \sim e^{i(kx_1 - \omega t)} \sim e^{i(k_r x_1 - \omega t)}\, e^{-k_i x_1}, \tag{7}$$

while a similar relationship exists for the out-of-plane displacement. Eq. (7) shows that the real part of the complex wavenumber, k_r, represents the propagating Lamb wave, while the imaginary part, k_i, is a measure of the attenuation of the amplitude of the displacement field due to material damping (k_i equal to zero corresponds to the linear elastic case).

The numerical algorithms used for the elastic case must be modified for the viscoelastic case because the elastic algorithms search for a frequency at a fixed *real* wavenumber. Coquin [13] showed that for small values of material damping—this is the case for the adhesive in this study—in a single plate, the real part of the wavenumber only changes slightly when compared to the corresponding elastic case. This behavior (that the dispersion curves for a viscoelastic case are nearly identical to those of the elastic case) is used to develop a linearization assumption of the matrix elements A_{ij} (presented in Appendix A) around the previously calculated linear elastic wavenumber, k_0, or

$$\hat{A}_{ij} = A_{ij}|_{(f_0,k_0)} + \left.\frac{\mathrm{d}A_{ij}}{\mathrm{d}k}\right|_{(f_0,k_0)} (\Delta k_r + \mathrm{i}k_i). \tag{8}$$

The shift in the real part of the wavenumber from the linear elastic wavenumber k_0 is quantified by Δk_r, while the attenuation contribution to the mode is given by k_i. The determinant of the linearized matrix, $\hat{A}$ is a complex polynomial, whose complex roots are determined with the symbolic manipulation program MAPLE. The number of complex roots at one linearization point is equal to the size of the matrix $\hat{A}$. The one root with the smallest shift Δk_r is the root of the propagating wave. The other roots are far away from the linearization point and are not physically realistic (the attenuation is so large that these waves will damp out for a realistic propagation distance), so they are discarded. One check of the validity of this solution procedure is to use the linearized matrix model of Eq. (8) to solve the three-layer *elastic* case of Section 2. The results give one root equal to zero (because there is no damping) and all of the other roots are complex conjugate, and are far away from the linearization point. These correspond to the 'physically unrealistic' roots neglected in the viscoelastic case.

Note that the linearization is not always realistic for small wavenumbers—the shift of the real wavenumber increases rapidly as the wavenumber approaches zero. As a result, any predicted attenuation values for wavenumbers less than 500 m^{-1} must be treated with caution. In addition, Eq. (7) shows that the imaginary wavenumber k_i must be zero or positive to describe a physically meaningful case, while the linearized matrix $\hat{A}$ yields roots with negative values for k_i in some cases. These negative k_i values represent damping for waves propagating in negative x_1-direction [14], so the attenuation of a wave is described by the absolute value of the imaginary wavenumber, k_i in the reminder of this paper.

The accuracy of this linearized viscoelastic model is tested by benchmarking with the attenuation curves of a single layer (stress free, viscoelastic plate) presented in Ref. [13] and obtaining exact agreement, see Ref. [9] for details. For reference purposes, Fig. 6 shows the attenuation curves, plus the corresponding dispersion curves for a single, stress free aluminum plate (0.9398 mm thick) with 'fictitious' material damping ($\nu' = -0.5$) added to the aluminum. Note that the shift in the real wavenumber is always much less than 1% of the wavenumber calculated for the linear elastic case—this shift is so small that it cannot even be seen in the dispersion curves of Fig. 6(b). Note that the wavenumbers plotted on the horizontal scales of Fig. 6 (and Fig. 7) are the real portion of Eq. (6), k_r, and represent the propagating portion of the wave. Since the shift in the wavenumber, Δk_r, is small in comparison to the linearization point, k_0, these k_r horizontal axes are effectively 'equal' to the k axes of the elastic cases.

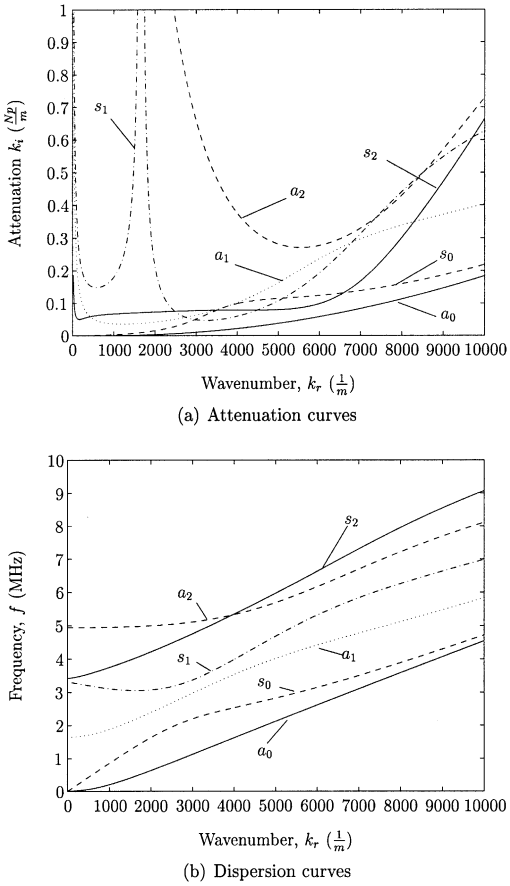

Fig. 6. Single aluminum plate adherend, with 'fictitious' damping added.

The analytical three-layer model described in Section 2 is modified by making the adhesive layer viscoelastic ($\nu' = -0.5$), while keeping the aluminum plates elastic—Fig. 7 shows the attenuation curves for the first eight modes, plus the corresponding dispersion curves, for this viscoelastic model. Since one objective of the current study is to understand the experimentally observed behavior of Ref. [1], the absolute value of damping in the adhesive layer is not critical. In fact, additional research [9] shows that for the

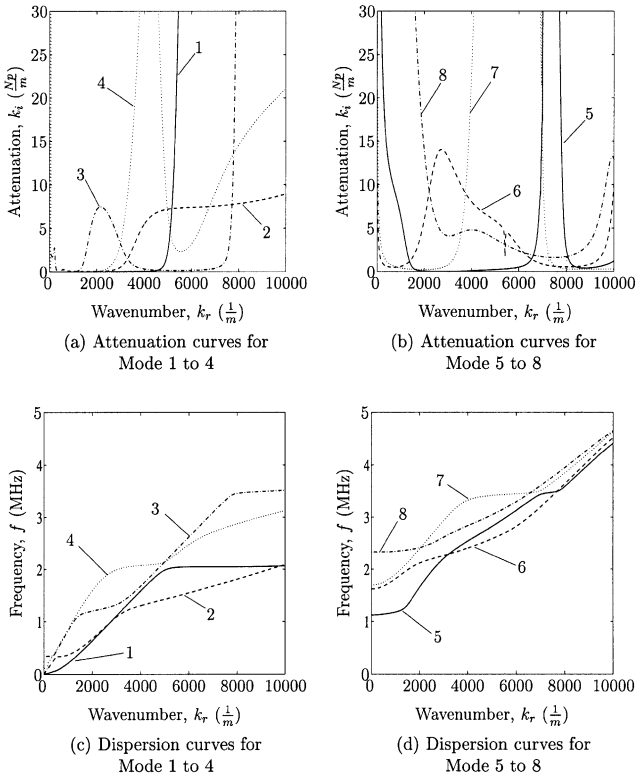

Fig. 7. Attenuation of the three-layer model with viscoelastic adhesive layer.

'low' level of damping considered in this study, the absolute damping values d' and s' only scale the attenuation curves of Fig. 7, and do not change their shape. These calculations also show that the damping values d' and s' only have a marginal influence on the real frequency–wavenumber relationship (dispersion) of the three-layer model—this is similar to the single plate case presented in Fig. 6.

The attenuation of the higher modes in both Figs. 6 and 7 is in general, higher than in the lower modes. This behavior, which is partially due to the frequency-dependent damping behavior of the Kelvin–Voight model, helps to explain the experimentally observed trend [1] that the higher modes of the adhesive bonded specimens are damped out. The attenuation curves of Fig. 7 show a number of trends for the three-layer model. First, when following along any of the eight modes, its 'aluminum' portion(s) have low attenuation, while its 'remaining' portion(s) have high attenuation values. In fact, the attenuation values of a particular mode decreases or increases as that mode approaches or recedes from its aluminum mode region(s). This corresponds to the fact that the displacements in the aluminum mode regions are dominated by the elastic, aluminum plates, while the displacements in the remaining regions of a mode mainly occur in the viscoelastic adhesive layer—this displacement behavior is shown in Fig. 4. In addition, the attenuation curves for the aluminum modes of this three-layer model generally follow the same trends as the attenuation curves of the single aluminum plate with fictitious damping. In other words, the combined attenuation behavior of a composite of the aluminum mode portions of these eight modes is similar to the attenuation behavior of the single viscoelastic plate shown in Fig. 6. Finally, attenuation is related to the shape of the dispersion curve in the 'transition' zones as a mode approaches or recedes from its aluminum mode region(s). There will be high attenuation if the dispersion curve has a gradual slope in this transition zone, because the adhesive layer displacements are dominant. If the transition zone is long, then the attenuation curve has a very smooth shape. If the transition zone is very short, then the attenuation curves increase very sharply.

The experiments in Ref. [1] also show that the amplitudes along the aluminum modes are lower in the two-layer specimen than in the three-layer specimen, so the attenuation behavior of the two-layer model is investigated. The two-layer attenuation curves show that the overall shape is the same for the two- and three-layer models, but the attenuation is higher in the two-layer model than in the three-layer model (see Ref. [9] for details). This behavior occurs because more energy propagates in the adhesive layer in the two-layer specimen than in the adhesive layer of the three-layer specimen—the energy in the three-layer specimen, must also propagate in the second aluminum plate, where there is no damping.

4. Finite element simulation

The analytical models do not calculate the absolute displacement values of the wave amplitudes, so these models cannot determine absolute amplitudes of the individual modes in the dispersion curves—yet these amplitudes are exactly the quantity measured in the experiments of Ref. [1]. Recall that the experimentally measured transient waveforms are operated on with the 2D-FFT to produce the dispersion relationships, and these dispersion curves are 3D plots with 'peak' heights directly related to signal amplitude (the absolute signal strength). Recent studies (e.g. see Ref. [17]) have shown that the FEM is capable of accurately and efficiently modeling guided wave propagation in the ultrasonic frequency range. An FEM simulation is robust, since an enormous amount of information (different data such as the time-dependent displacements at multiple locations, including interior points) can be collected in a single simulation. This research uses the FEM code, ABAQUS/Explicit [18].

The spatial discretization of a specimen is a critical issue when modeling wave propagation with the FEM—an accurate representation requires that the smallest wavelength be discretized with at least 20 nodes [17]. Unfortunately, an accurate discretization of the three-layer specimen for a maximum frequency of 5 MHz, requires 6.35 million elements [9]. Such a model is dominated by the fine discretization needed to model wave propagation in the adhesive

layer. The objective of the FEM simulation is to understand trends and behavior and not necessarily to wholly model the two- and three-layer adhesive bonded specimens. As a result, a coarser model that does not accurately describe modes with very short wavelengths (high frequency components) that *can* occur in the adhesive bond is acceptable—these modes are not measured in the experiments of Ref. [1] so they are only of minor interest in this research. This research uses a four-node plane-strain continuum element (CPE4R). Such an element provides a second-order interpolation, with reduced integration and hourglass control (hourglassing is a numerical phenomena by which a zero-energy mode propagates [18]). Each node has two-degrees of freedom (plane-strain assumption). An FEM model is developed with a mesh of 140 000 elements and an element size of 0.03–0.05 mm (three-layer specimen). A mesh refinement of a factor of 2 (that increases the problem size by a factor of 4) produces the same solution—this defines convergence of the FEM model [17].

Infinite elements are attached at the ends of the FEM model to absorb the incoming energy and simulate an infinite specimen, thus eliminating most of the reflections from the edges. The 'laser' source is located 25 mm away from the edge and is simulated as a force in the out-of-plane (x_2-direction), distributed as a sine over a time of 0.3 μs which corresponds to a frequency of 3.3 MHz. The particle velocities (time-derivative of displacements) are 'measured' on the surface for 200 points, which are equally spaced from 30.15 to 60.15 mm ($\Delta x = 0.15$ mm) away from the source. The FEM simulation uses 200 spatial points (both in-plane and out-of-plane) for the 2D-FFT (compared to the 50 spatial points of the experiments) to achieve superior spatial resolution. By measuring both velocity components, it is possible to investigate the relative mode strengths of the in-plane and out-of-plane amplitudes. The same measurements are also completed on interior planes that are parallel to the surface to investigate the strength of the modes inside of the specimen. The measured data is processed (in a similar fashion to the experiments of Ref. [1]) with a 2D-FFT implemented in MATLAB. The 2D-FFT routine operates on this set of 200 equally spaced, transient waveforms by computing a temporal Fourier transform (time to frequency domain) followed by a spatial Fourier transform (position to wavenumber domain). There is no windowing; the temporal FFT operates on the entire transient waveform, and each of these 200 frequency domain signals (in their entirety) are used in the spatial FFT.

The first simulations are done without damping, by assuming that the adhesive is linear elastic. Next, damping is added to the adhesive layer to simulate its viscoelastic behavior. Damping is added in ABAQUS using a strain proportional damping (unit of time) that describes viscous material damping which causes a 'damping stress' in the adhesive which is proportional to the strain rate. This is similar to the viscous stress–strain relationship of the Kelvin–Voight solid in Eq. (1). Fig. 8 shows the dispersion

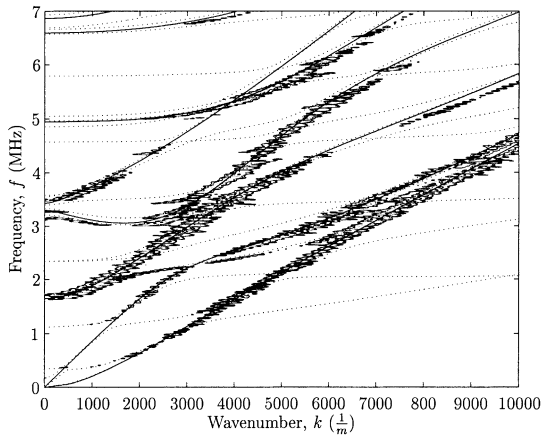

(a) In-plane component

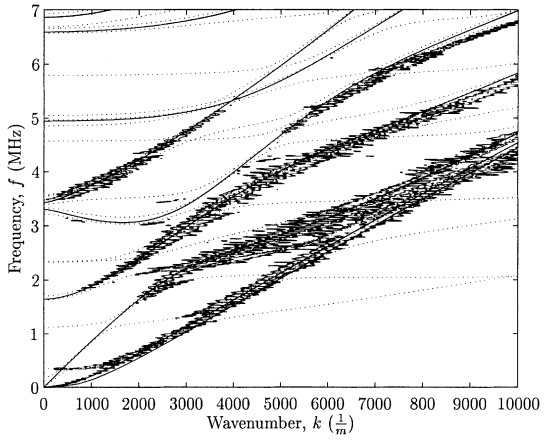

(b) Out-of-plane component

Fig. 8. FEM simulation of three-layer model, elastic adhesive layer. This includes the analytical dispersion curves of the three-layer model (dotted lines) and a single aluminum plate adherend (solid lines).

curves developed with a 2D-FFT of the in-plane and out-of-plane surface velocities, for an FEM simulation of the three-layer specimen with an elastic adhesive layer (no damping). In addition, Fig. 8 includes the analytical solution for the dispersion curves of the three-layer specimen calculated with the analytical model (plotted as dotted lines), plus the analytical solution for a single, stress free aluminum plate adherend (plotted as solid lines). Fig. 8 shows that the primary motion is—as measured in the experiments and predicted by the analytical model—along the aluminum modes. However, there are also some modes visible at the transition zones near the aluminum modes. These are 'non-aluminum modes' that are not measured in the experiments, but are predicted by the analytical model. Overall, the out-of-plane motion is stronger (higher amplitudes) than the in-plane motion, but the transition zones are better defined in the in-plane plot.

Fig. 9 shows the 2D-FFT of the same FEM simulation, except that the adhesive layer is viscoelastic (damping added). The material damping has the effect that only

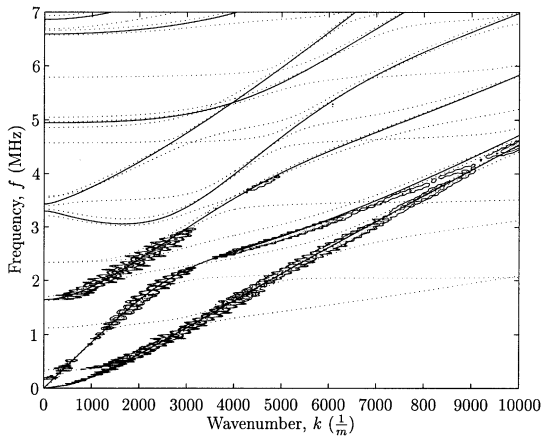

(a) In-plane component

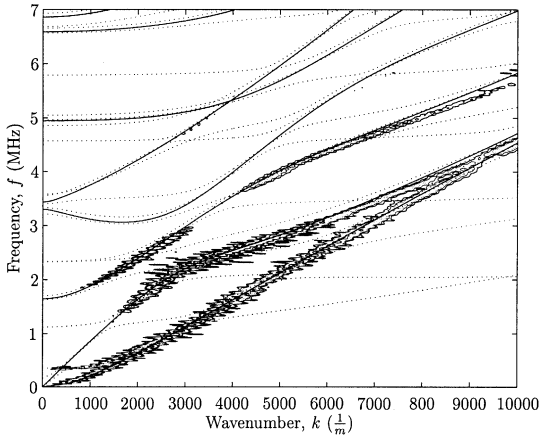

(b) Out-of-plane component

Fig. 9. FEM simulation of three-layer model, viscoelastic adhesive layer. This includes the analytical dispersion curves of the three-layer model (dotted lines) and a single aluminum plate adherend (solid lines).

displacements along the aluminum modes are visible, and any traces of a mode in the transition zones are no longer visible. In addition, some of the higher aluminum modes, that are clearly visible in Fig. 8, are damped out in Fig. 9. Damping along the aluminum modes is strongest in the vicinity of the transition to its non-aluminum (motion in the adhesive) portion. In fact, the size of these gaps may be a possible experimentally measurable metric to determine the quality of a bond.

Finally, one special mode is the first 'horizontal mode,' with a cut-off frequency of around 350 kHz. This mode is clearly visible in both the damped and un-damped simulations (out-of-plane, in Figs. 8 and 9) for wavenumbers below 1000 m^{-1}. Note that an inspection of the theoretical dispersion curves in this region (as presented in Figs. 3 and 7(c)) shows that this horizontal mode is mode 2 (and a small part of mode 4). The analytical eigenvectors of mode 2 at wavenumbers $k = 500$ and 1000 m^{-1} reveals that there are significant out-of-plane displacements in the aluminum plates and in the adhesive layer at these wavenumbers. This is different from the previous analytical results (as presented in Fig. 4)—this mode does not follow a single plate mode at these wavenumbers (it is not an aluminum mode), yet it has significant displacements in the aluminum plates at these wavenumbers. An explanation for this behavior is that the motion of the adhesive layer is so dominant in this region that it causes significant displacements in the aluminum plates. In addition, material damping has a small effect in this region (due in part to the frequency-dependent nature of the Kelvin–Voight model), so there is little difference between the damped and un-damped results in Figs. 8 and 9. This trend is reinforced when considering the attenuation curve for mode 2 in Fig. 7(a)—there is very little attenuation in mode 2 in this region. This mode is important for NDE applications—it is not dominated by the motion of the aluminum plates at these wavenumbers, so it should be very sensitive to the properties of the adhesive layer. It is important to note that this mode was only identified and interpreted after considering both the FEM and analytical results.

5. Conclusion

This research uses analytical and computational models to develop a quantitative understanding of the propagation of guided Lamb waves in multi-layered, adhesive bonded components—this study provides a theoretical understanding of the experimental behavior observed in Ref. [1].

The analytical two- and three-layer models show that only modes in the vicinity of the single aluminum plate modes (and not the additional modes) have substantial displacements (both in-plane and out-of-plane) on the surface of the aluminum adherends. As a result, the experimental measurements in Ref. [1] only see these aluminum modes—this is one reason why the experimental results for a three-layer bonded specimen in Fig. 1 only show some of the modes of a single, 0.9398 mm thick aluminum plate. The displacement fields show that regions removed from the aluminum modes only have substantial displacements in the adhesive layer, and not in the aluminum plate adherends. The aluminum modes have similar displacement fields to those of a single, stress free aluminum plate. The results of the two-layer model are similar to the results of the three-layer model, except that there is only one mode following the aluminum modes in the two-layer model.

The attenuation values of a particular mode decrease or increase as that mode approaches or recedes from its aluminum mode region(s). This corresponds to the fact that the displacements in the aluminum mode regions are dominated by the elastic, aluminum plates, while the displacements in the remaining regions of a mode mainly occur in the viscoelastic adhesive layer. The shapes of the attenuation curves for the three-layer model along the aluminum modes are very similar to the attenuation of a single, stress free aluminum plate with fictitious damping. The two-layer attenua-

tion curves show that attenuation is higher in the two-layer model than in the three-layer model. This behavior occurs because more energy propagates in the adhesive layer in the two-layer specimen than in the adhesive layer of the three-layer specimen.

The FEM simulation is very robust, producing an enormous amount of data in a single 'numerical experiment'. These results agree with the predictions of the analytical model and the experimental results—the primary motion is along the aluminum modes. The addition of material damping to the adhesive layer has the effect that only displacements along the aluminum modes are visible. In addition, some of the higher aluminum modes that are clearly visible in the elastic case are damped out by the viscoelastic adhesive. A combination of the analytical model, transient FEM simulation and experimental measurements provides an excellent understanding of the guided wave's behavior in an adhesive bonded, layered waveguide.

Acknowledgements

The Deutscher Akademischer Austausch Dienst (DAAD) provided partial support to Robert Seifried.

Appendix A

The system of 12 equations for the three-layer case can be written in matrix form as

$$\underbrace{\begin{bmatrix} A_{1,1} & A_{1,2} & \cdots & A_{1,12} \\ A_{2,1} & A_{2,2} & \cdots & A_{2,12} \\ \vdots & \vdots & \ddots & \vdots \\ A_{12,1} & A_{12,2} & \cdots & A_{12,12} \end{bmatrix}}_{\boldsymbol{A}} \underbrace{\begin{bmatrix} C_1^{(1)} \\ C_2^{(1)} \\ \vdots \\ C_4^{(4)} \end{bmatrix}}_{\boldsymbol{C}} = \begin{bmatrix} 0 \\ 0 \\ \vdots \\ 0 \end{bmatrix} \tag{A1}$$

The elements of the matrix **A** are shown using the notation of Ref. [2]. First, consider the boundary condition at the top surface ($x_2 = 0$) of $\sigma_{22}^{(1)} = 0$. This yields

$$A_{1,1} = \lambda^{(1)} K_{\mathrm{L}}^{(1)2} + \mu^{(1)} k_{\mathrm{L}}^{(1)2}, \qquad A_{1,2} = \lambda^{(1)} K_{\mathrm{L}}^{(1)2} + \mu^{(1)} k_{\mathrm{L}}^{(1)2},$$

$$A_{1,3} = -2\mu^{(1)} k K_{\mathrm{T}}^{(1)}, \qquad A_{1,4} = 2\mu^{(1)} k K_{\mathrm{T}}^{(1)},$$

$$A_{1,m} = 0 \qquad \text{for } 5 \leqq m \leqq 12, \tag{A2}$$

where the superscript (n) is the layer number, and $K_{\mathrm{L}}^{(n)}$ and $K_{\mathrm{T}}^{(n)}$ are the orthogonal wavenumbers (real or complex). The wavenumber k is parallel to the propagation direction, and related to the orthogonal wavenumbers by

$$K_{\mathrm{L}}^{(n)} = \sqrt{k_{\mathrm{L}}^{(n)2} - k^2}, \tag{A3}$$

$$K_{\mathrm{T}}^{(n)} = \sqrt{k_{\mathrm{T}}^{(n)2} - k^2}. \tag{A4}$$

The second boundary condition on the upper surface, $\sigma_{12}^{(1)} = 0$, yields

$$A_{2,1} = -2\mu^{(1)} k K_{\mathrm{L}}^{(1)}, \qquad A_{2,2} = 2\mu^{(1)} k K_{\mathrm{L}}^{(1)},$$

$$A_{2,3} = \mu^{(1)}\left(K_{\mathrm{T}}^{(1)2} - k^2\right), \qquad A_{2,4} = \mu^{(1)}\left(K_{\mathrm{T}}^{(1)2} - k^2\right),$$

$$A_{2,m} = 0 \qquad \text{for } 5 \leqq m \leqq 12. \tag{A5}$$

The first traction boundary condition for interface 1 at $x_2 = h_1$ requires that the normal tractions, $\sigma_{22}^{(1)}$ and $\sigma_{22}^{(2)}$ be equal, or

$$A_{3,1} = -\left(\lambda^{(1)} K_{\mathrm{L}}^{(1)2} + \mu^{(1)} k_{\mathrm{L}}^{(1)2}\right) \mathrm{e}^{\mathrm{i}K_{\mathrm{L}}^{(1)} h_1},$$

$$A_{3,2} = -\left(\lambda^{(1)} K_{\mathrm{L}}^{(1)2} + \mu^{(1)} k_{\mathrm{L}}^{(1)2}\right) \mathrm{e}^{-\mathrm{i}K_{\mathrm{L}}^{(1)} h_1},$$

$$A_{3,3} = -2\mu^{(1)} k K_{\mathrm{T}}^{(1)} \, \mathrm{e}^{\mathrm{i}K_{\mathrm{T}}^{(1)} h_1}, \qquad A_{3,4} = 2\mu^{(1)} k K_{\mathrm{T}}^{(1)} \, \mathrm{e}^{-\mathrm{i}K_{\mathrm{T}}^{(1)} h_1},$$

$$A_{3,5} = \left(\lambda^{(2)} K_{\mathrm{L}}^{(2)2} + \mu^{(2)} k_{\mathrm{L}}^{(2)2}\right) \mathrm{e}^{\mathrm{i}K_{\mathrm{L}}^{(2)} h_1},$$

$$A_{3,6} = \left(\lambda^{(2)} K_{\mathrm{L}}^{(2)2} + \mu^{(2)} k_{\mathrm{L}}^{(2)2}\right) \mathrm{e}^{-\mathrm{i}K_{\mathrm{L}}^{(2)} h_1},$$

$$A_{3,7} = 2\mu^{(2)} k K_{\mathrm{T}}^{(2)} \, \mathrm{e}^{\mathrm{i}K_{\mathrm{T}}^{(2)} h_1}, \qquad A_{3,8} = -2\mu^{(2)} k K_{\mathrm{T}}^{(2)} \, \mathrm{e}^{-\mathrm{i}K_{\mathrm{T}}^{(2)} h_1},$$

$$A_{3,m} = 0 \qquad \text{for } 9 \leqq m \leqq 12. \tag{A6}$$

The second traction boundary condition at interface 1 is $\sigma_{12}^{(1)} = \sigma_{12}^{(2)}$, or

$$A_{4,1} = -2\mu^{(1)} k K_{\mathrm{L}}^{(1)} \, \mathrm{e}^{\mathrm{i}K_{\mathrm{L}}^{(1)} h_1}, \qquad A_{4,2} = 2\mu^{(1)} k K_{\mathrm{L}}^{(1)} \, \mathrm{e}^{-\mathrm{i}K_{\mathrm{L}}^{(1)} h_1},$$

$$A_{4,3} = \mu^{(1)}\left(K_{\mathrm{T}}^{(1)2} - k^2\right) \mathrm{e}^{\mathrm{i}K_{\mathrm{T}}^{(1)} h_1},$$

$$A_{4,4} = \mu^{(1)}\left(K_{\mathrm{T}}^{(1)2} - k^2\right) \mathrm{e}^{-\mathrm{i}K_{\mathrm{T}}^{(1)} h_1},$$

$$A_{4,5} = 2\mu^{(2)} k K_{\mathrm{L}}^{(2)} \, \mathrm{e}^{\mathrm{i}K_{\mathrm{L}}^{(2)} h_1}, \qquad A_{4,6} = -2\mu^{(2)} k K_{\mathrm{L}}^{(2)} \, \mathrm{e}^{-\mathrm{i}K_{\mathrm{L}}^{(2)} h_1},$$

$$A_{4,7} = -\mu^{(2)}\left(K_{\mathrm{T}}^{(2)2} - k^2\right) \mathrm{e}^{\mathrm{i}K_{\mathrm{T}}^{(2)} h_1},$$

$$A_{4,8} = -\mu^{(2)}\left(K_{\mathrm{T}}^{(2)2} - k^2\right) \mathrm{e}^{-\mathrm{i}K_{\mathrm{T}}^{(2)} h_1},$$

$$A_{4,m} = 0 \qquad \text{for } 9 \leqq m \leqq 12. \tag{A7}$$

The first displacement boundary for interface 1 ($x_2 = h_1$) is continuous horizontal displacements, $u_1^{(1)} = u_1^{(2)}$, or

$$A_{5,1} = k \, \mathrm{e}^{\mathrm{i}K_{\mathrm{L}}^{(1)} h_1}, \qquad A_{5,2} = k \, \mathrm{e}^{-\mathrm{i}K_{\mathrm{L}}^{(1)} h_1},$$

$$A_{5,3} = -K_{\mathrm{T}}^{(1)} \, \mathrm{e}^{\mathrm{i}K_{\mathrm{T}}^{(1)} h_1}, \qquad A_{5,4} = K_{\mathrm{T}}^{(1)} \, \mathrm{e}^{-\mathrm{i}K_{\mathrm{T}}^{(1)} h_1},$$

$$A_{5,5} = -k \, \mathrm{e}^{\mathrm{i}K_{\mathrm{L}}^{(2)} h_1}, \qquad A_{5,6} = -k \, \mathrm{e}^{-\mathrm{i}K_{\mathrm{L}}^{(2)} h_1},$$

$$A_{5,7} = K_{\mathrm{T}}^{(2)} \, \mathrm{e}^{\mathrm{i}K_{\mathrm{T}}^{(2)} h_1}, \qquad A_{5,8} = -K_{\mathrm{T}}^{(2)} \, \mathrm{e}^{-\mathrm{i}K_{\mathrm{T}}^{(2)} h_1},$$

$$A_{5,m} = 0 \qquad \text{for } 9 \leqq m \leqq 12. \tag{A8}$$

The second displacement boundary condition at interface 1

is $u_2^{(1)} = u_2^{(2)}$, or

$$A_{6,1} = K_{\mathrm{L}}^{(1)}\,\mathrm{e}^{\mathrm{i}K_{\mathrm{L}}^{(1)}h_1}, \qquad A_{6,2} = -K_{\mathrm{L}}^{(1)}\,\mathrm{e}^{-\mathrm{i}K_{\mathrm{L}}^{(1)}h_1},$$

$$A_{6,3} = k\,\mathrm{e}^{\mathrm{i}K_{\mathrm{T}}^{(1)}h_1}, \qquad A_{6,4} = k\,\mathrm{e}^{-\mathrm{i}K_{\mathrm{T}}^{(1)}h_1},$$

$$A_{6,5} = -K_{\mathrm{L}}^{(2)}\,\mathrm{e}^{\mathrm{i}K_{\mathrm{L}}^{(2)}h_1}, \qquad A_{6,6} = K_{\mathrm{L}}^{(2)}\,\mathrm{e}^{-\mathrm{i}K_{\mathrm{L}}^{(2)}h_1},$$

$$A_{6,7} = -k\,\mathrm{e}^{\mathrm{i}K_{\mathrm{T}}^{(2)}h_1}, \qquad A_{6,8} = -k\,\mathrm{e}^{-\mathrm{i}K_{\mathrm{T}}^{(2)}h_1},$$

$$A_{6,m} = 0 \qquad \text{for } 9 \leqq m \leqq 12. \tag{A9}$$

The first traction boundary condition at interface 2 ($x_2 = h_2$) is $\sigma_{22}^{(2)} = \sigma_{22}^{(3)}$, or

$$A_{7,m} = 0 \qquad \text{for } 1 \leqq m \leqq 4,$$

$$A_{7,5} = -\left(\lambda^{(2)}K_{\mathrm{L}}^{(2)2} + \mu^{(2)}k_{\mathrm{L}}^{(2)2}\right)\mathrm{e}^{\mathrm{i}K_{\mathrm{L}}^{(2)}h_2},$$

$$A_{7,6} = -\left(\lambda^{(2)}K_{\mathrm{L}}^{(2)2} + \mu^{(2)}k_{\mathrm{L}}^{(2)2}\right)\mathrm{e}^{-\mathrm{i}K_{\mathrm{L}}^{(2)}h_2},$$

$$A_{7,7} = -2\mu^{(2)}kK_{\mathrm{T}}^{(2)}\,\mathrm{e}^{\mathrm{i}K_{\mathrm{T}}^{(2)}h_2}, \qquad A_{7,8} = 2\mu^{(2)}kK_{\mathrm{T}}^{(2)}\,\mathrm{e}^{-\mathrm{i}K_{\mathrm{T}}^{(2)}h_2},$$

$$A_{7,9} = \left(\lambda^{(3)}K_{\mathrm{L}}^{(3)2} + \mu^{(3)}k_{\mathrm{L}}^{(3)2}\right)\mathrm{e}^{\mathrm{i}K_{\mathrm{L}}^{(3)}h_2},$$

$$A_{7,10} = \left(\lambda^{(3)}K_{\mathrm{L}}^{(3)2} + \mu^{(3)}k_{\mathrm{L}}^{(3)2}\right)\mathrm{e}^{-\mathrm{i}K_{\mathrm{L}}^{(3)}h_2},$$

$$A_{7,11} = 2\mu^{(3)}kK_{\mathrm{T}}^{(3)}\,\mathrm{e}^{\mathrm{i}K_{\mathrm{T}}^{(3)}h_2}, \qquad A_{7,12} = -2\mu^{(3)}kK_{\mathrm{T}}^{(3)}\,\mathrm{e}^{-\mathrm{i}K_{\mathrm{T}}^{(3)}h_2}. \tag{A10}$$

The second traction boundary condition at interface 2 is $\sigma_{12}^{(2)} = \sigma_{12}^{(3)}$, or

$$A_{8,m} = 0 \qquad \text{for } 1 \leqq m \leqq 4,$$

$$A_{8,5} = -2\mu^{(2)}kK_{\mathrm{L}}^{(2)}\,\mathrm{e}^{\mathrm{i}K_{\mathrm{L}}^{(2)}h_2},$$

$$A_{8,6} = 2\mu^{(2)}kK_{\mathrm{L}}^{(2)}\,\mathrm{e}^{-\mathrm{i}K_{\mathrm{L}}^{(2)}h_2},$$

$$A_{8,7} = \mu^{(2)}\left(K_{\mathrm{T}}^{(2)2} - k^2\right)\mathrm{e}^{\mathrm{i}K_{\mathrm{T}}^{(2)}h_2},$$

$$A_{8,8} = \mu^{(2)}\left(K_{\mathrm{T}}^{(2)2} - k^2\right)\mathrm{e}^{-\mathrm{i}K_{\mathrm{T}}^{(2)}h_2},$$

$$A_{8,9} = 2\mu^{(3)}kK_{\mathrm{L}}^{(3)}\,\mathrm{e}^{\mathrm{i}K_{\mathrm{L}}^{(3)}h_2},$$

$$A_{8,10} = -2\mu^{(3)}kK_{\mathrm{L}}^{(3)}\,\mathrm{e}^{-\mathrm{i}K_{\mathrm{L}}^{(3)}h_2},$$

$$A_{8,11} = -\mu^{(3)}\left(K_{\mathrm{T}}^{(3)2} - k^2\right)\mathrm{e}^{\mathrm{i}K_{\mathrm{T}}^{(3)}h_2},$$

$$A_{8,12} = -\mu^{(3)}\left(K_{\mathrm{T}}^{(3)2} - k^2\right)\mathrm{e}^{-\mathrm{i}K_{\mathrm{T}}^{(3)}h_2}. \tag{A11}$$

The first displacement boundary condition at interface 2 is $u_1^{(2)} = u_1^{(3)}$, or

$$A_{9,m} = 0 \qquad \text{for } 1 \leqq m \leqq 4,$$

$$A_{9,5} = k\,\mathrm{e}^{\mathrm{i}K_{\mathrm{L}}^{(2)}h_2}, \qquad A_{9,6} = k\,\mathrm{e}^{-\mathrm{i}K_{\mathrm{L}}^{(2)}h_2},$$

$$A_{9,7} = -K_{\mathrm{T}}^{(2)}\,\mathrm{e}^{\mathrm{i}K_{\mathrm{T}}^{(2)}h_2}, \qquad A_{9,8} = K_{\mathrm{T}}^{(2)}\,\mathrm{e}^{-\mathrm{i}K_{\mathrm{T}}^{(2)}h_2},$$

$$A_{9,9} = -k\,\mathrm{e}^{\mathrm{i}K_{\mathrm{L}}^{(3)}h_2}, \qquad A_{9,10} = -k\,\mathrm{e}^{-\mathrm{i}K_{\mathrm{L}}^{(3)}h_2},$$

$$A_{9,11} = K_{\mathrm{T}}^{(3)}\,\mathrm{e}^{\mathrm{i}K_{\mathrm{T}}^{(3)}h_2}, \qquad A_{9,12} = -K_{\mathrm{T}}^{(3)}\,\mathrm{e}^{-\mathrm{i}K_{\mathrm{T}}^{(3)}h_2}. \tag{A12}$$

The second displacement boundary condition at interface 2 is $u_2^{(2)} = u_2^{(3)}$

$$A_{10,m} = 0 \qquad \text{for } 1 \leqq m \leqq 4,$$

$$A_{10,5} = K_{\mathrm{L}}^{(2)}\,\mathrm{e}^{\mathrm{i}K_{\mathrm{L}}^{(2)}h_2}, \qquad A_{10,6} = -K_{\mathrm{L}}^{(2)}\,\mathrm{e}^{-\mathrm{i}K_{\mathrm{L}}^{(2)}h_2},$$

$$A_{10,7} = k\,\mathrm{e}^{\mathrm{i}K_{\mathrm{T}}^{(2)}h_2}, \qquad A_{10,8} = k\,\mathrm{e}^{-\mathrm{i}K_{\mathrm{T}}^{(2)}h_2},$$

$$A_{10,9} = -K_{\mathrm{L}}^{(3)}\,\mathrm{e}^{\mathrm{i}K_{\mathrm{L}}^{(3)}h_2}, \qquad A_{10,10} = K_{\mathrm{L}}^{(3)}\,\mathrm{e}^{-\mathrm{i}K_{\mathrm{L}}^{(3)}h_2},$$

$$A_{10,11} = -k\,\mathrm{e}^{\mathrm{i}K_{\mathrm{T}}^{(3)}h_2}, \qquad A_{10,12} = -k\,\mathrm{e}^{-\mathrm{i}K_{\mathrm{T}}^{(3)}h_2}. \tag{A13}$$

The final boundary conditions are on the stress free lower surface ($x_2 = h_3$), $\sigma_{22}^{(3)} = 0$

$$A_{11,m} = 0 \qquad \text{for } 1 \leqq m \leqq 8,$$

$$A_{11,9} = \left(\lambda^{(3)}K_{\mathrm{L}}^{(3)2} + \mu^{(3)}k_{\mathrm{L}}^{(3)2}\right)\mathrm{e}^{\mathrm{i}K_{\mathrm{L}}^{(3)}h_3},$$

$$A_{11,10} = \left(\lambda^{(3)}K_{\mathrm{L}}^{(3)2} + \mu^{(3)}k_{\mathrm{L}}^{(3)2}\right)\mathrm{e}^{-\mathrm{i}K_{\mathrm{L}}^{(3)}h_3},$$

$$A_{11,11} = 2\mu^{(3)}kK_{\mathrm{T}}^{(3)}\,\mathrm{e}^{\mathrm{i}K_{\mathrm{T}}^{(3)}h_3},$$

$$A_{11,12} = -2\mu^{(3)}kK_{\mathrm{T}}^{(3)}\,\mathrm{e}^{\mathrm{i}K_{\mathrm{T}}^{(3)}h_3}. \tag{A14}$$

The last boundary condition $\sigma_{12}^{(3)} = 0$ at the lower surface gives

$$A_{12,m} = 0 \qquad \text{for } 1 \leqq m \leqq 8,$$

$$A_{12,9} = -2\mu^{(3)}kK_{\mathrm{L}}^{(3)}\,\mathrm{e}^{\mathrm{i}K_{\mathrm{L}}^{(3)}h_3},$$

$$A_{12,10} = 2\mu^{(3)}kK_{\mathrm{L}}^{(3)}\,\mathrm{e}^{-\mathrm{i}K_{\mathrm{L}}^{(3)}h_3},$$

$$A_{12,11} = \mu^{(3)}\left(K_{\mathrm{T}}^{(3)2} - k^2\right)\mathrm{e}^{\mathrm{i}K_{\mathrm{T}}^{(3)}h_3}$$

$$A_{12,12} = \mu^{(3)}\left(K_{\mathrm{T}}^{(3)2} - k^2\right)\mathrm{e}^{-\mathrm{i}K_{\mathrm{T}}^{(3)}h_3}. \tag{A15}$$

References

[1] Heller K, Jacobs LJ, Qu J. Characterization of adhesive bond properties using Lamb waves. NDT E Int 2000;33:555–63.

[2] Rose JL. Ultrasonic waves in solid media. Cambridge: Cambridge University Press, 1999.

[3] Lowe MJS, Cawley P. The applicability of plate wave techniques for the inspection of adhesive and diffusion bonded joints. J Nondestruct Eval 1994;13(4):185–200.

[4] Nagy PB, Adler L. Nondestructive evaluation of adhesive joints by guided waves. J Appl Phys 1989;66(10):4658–63.

[5] Lowe MJS, Challis RE, Chan CW. The transmission of Lamb waves across adhesively bonded lap joints. J Acoust Soc Am 2000;107(3):1333–45.

[6] Mal AK, Xu PC, Bar-Cohen Y. Analysis of leaky Lamb waves in bonded plates. Int J Engng Sci 1989;27(7):779–91.

[7] Pavlakovic BN, Lowe MJS, Alleyne DN, Cawley P. Disperse: a general purpose program for creating dispersion curves. In: Thompson DO, Chimenti DE, editors. Review of progress in quantitative NDE, vol. 16. New York: Plenum Press, 1997. p. 185–92.

[8] Niklasson AJ, Datta SK. On the modeling of guided waves in plates with thin superconducting layers. In: Thompson DO, Chimenti DE, editors. Review of progress in quantitative NDE, vol. 19A. New York: American Institute of Physics, 2000. p. 185–92.

[9] Seifried R. Propagation of guided waves in adhesive bonded components. MS Thesis, Engineering Science and Mechanics. Atlanta: Georgia Institute of Technology, 2000.

[10] Jarzynski J. Mechanisms of sound attenuation in materials. In: Corsaro RD, Sperling LH, editors. Sound and vibration damping with polymers, vol. 424. Washington, DC: American Chemical Society, 1990. p. 166–207.

[11] Seifried R, Jacobs LJ, Qu J. Characterization of adhesive bond properties with Lamb waves. In: Thompson DO, Chimenti DE, editors. Review of progress in quantitative NDE, vol. 20B. New York: American Institute of Physics, 2001. p. 1074–81.

[12] Nayfeh AH, Nagy PB. Excess attenuation of leaky Lamb waves due to viscous fluid loading. J Acoust Soc Am 1997;101(5):2649–58.

[13] Coquin GA. Attenuation of guided waves in isotropic viscoelastic materials. J Acoust Soc Am 1964;36(6):1074–80.

[14] Chervinko OP, Senchenkov IK. Harmonic viscoelastic waves in a layer and in an infinite cylinder. Sov Appl Mech 1986;22(12):1136–41.

[15] Bonnin A, Huchon R, Deschamps M. Ultrasonic waves propagating in absorbing thin plates: application to paper characterization. Ultrasonics 2000;37:555–63.

[16] Dalton RP, Lowe MJS, Cawley P. Propagation of guided waves in aircraft structures. In: Thompson DO, Chimenti DE, editors. Review of progress in quantitative NDE, vol. 19. New York: Plenum, 1999. p. 225–32.

[17] Moser F, Jacobs LJ, Qu J. Modeling elastic wave propagation in waveguides with the finite element method. NDT E Int 1999;32:225–34.

[18] ABAQUS/Explicit version 5.6: users manual, theory manual, example problems manual, 1996.